*ISSN 1392-1207. MECHANIKA. Vol. 30, No. 1, 2024: 5–13*

# The Characterization of the Plastic Instability of S235 Thin Steel Sheets by Multiple Regression and Analysis of Variance Methods

**Nejib GHAZOUANI*, Mohamed Toumi NASRI**, ***, Boulbaba ELADEB*, Wael SALAH*, Mohammed A. TASHKANDI*, Nidhal BECHEIKH***

**College of Engineering, Northern Border University, PO Box 1321 Arar, Northern Borders 73222, Saudi Arabia, E-mails: nejib.ghazouani@nbu.edu.sa, aboulbaba.eladeb@nbu.edu.sa , wael.khalil@nbu.edu.sa, mohammd.tashkandi@nbu.edu.sa, nidhal.becheikh@nbu.edu.sa*

***LMPE (LR18ES01), Ecole Nationale Supérieure d'Ingénieurs de Tunis (ENSIT), Université de Tunis, 5 Av. Taha Hussein, Montfleury 1008 Tunis, Tunisia, E-mail: nasri.medtoumi@gmail.com*

****National Engineering School of BIZERTE, University of Carthage, BP66, Menzel Abderrahman University Campus 7035, Bizerte, Tunisia*

https://doi.org/10.5755/j02.mech.34036

## 1. Introduction

Sheet metal forming is a fundamental process in many industrial applications, from automotive to aerospace engineering. Understanding the behavior of metals undergoing forming processes is crucial for predicting and controlling the quality of the final product. In particular, the onset of plastic instability can lead to defects and failure in the formed parts [1, 2]. Therefore, accurate characterization and prediction of plastic instability is of utmost importance.

The S235 steel, commonly used in sheet metal forming, presents unique challenges due to its complex anisotropy, elastoplastic and damage behaviors. This study aims to provide a comprehensive characterization of the plastic instability of S235 thin steel sheets using a novel identification method.

The study of metal plasticity and the prediction of plastic instability has been an area of active research for many years [3]. Plastic instability in sheet metals during forming processes can lead to undesirable outcomes such as wrinkling, tearing, and other forms of deformation that can compromise the integrity of the final product [4]. The ability to predict and control the onset of plastic instability is therefore of great interest in the field of materials science and engineering [5].

The mechanical behavior of metals, including plastic deformation and failure, has been traditionally characterized using uniaxial tensile tests [6]. However, this method does not capture the biaxial stress state that occurs in sheet metal forming processes [7]. To address this, hydraulic bulge tests have been used as a means to generate biaxial stress conditions in sheet materials. The bulge test method has been extensively studied and used to characterize a wide range of materials, including aluminum alloys [8], dual-phase steels [9], and stainless steels.

The S235 steel, in particular, has been widely used in various applications due to its excellent mechanical properties. Research on S235 steel has focused on understanding its behavior under different loading conditions. For example, a study by Davis et al. investigated the anisotropic behavior of S235 steel under various loading conditions, providing valuable insights into the material's directional properties [10].

In recent years, the application of statistical methods such as analysis of variance (ANOVA) and regression analysis has gained popularity in the field of materials science. These methods have been used to identify and quantify the significant factors affecting the material behavior [11]. Furthermore, finite element simulations have been extensively used for predicting the behavior of materials under various forming conditions, and for validating experimental results [12].

In this study, we aim to build upon this body of research and present a new identification method for characterizing the elastoplastic damage behavior of S235 steel sheets [13]. Our method combines the use of bulge tests, ANOVA, multiple regression, and finite element simulations to provide a comprehensive characterization of the plastic instability of S235 steel sheets [14, 15, 16].

Our approach uses the analysis of variance (ANOVA) and multiple regression methods to identify parameters that characterize the elastoplastic damage behavior of the sheet metal [17,18,19]. The method was applied to both experimental and numerical simulation results of a bulge test on the S235 steel sheets. The numerical simulations were performed using the finite element method, a powerful tool for predicting the behavior of materials under various loading conditions [20, 21].

The identified models were validated through a comparison with experimental results on several hydroforming applications, including free expansion and expansion in matrix cavities. This validation process demonstrated a high degree of coherence between the experimental observations and the numerical predictions of instabilities.

In this paper, we present in detail the methodology of the identification process, the experimental and numerical results, and the validation of the identified models. We also discuss the implications of the investigation findings for the prediction and control of plastic instability in sheet metal forming processes.

The remainder of this paper is organized as follows: Section 2 provides background information on the S235 steel and its importance in sheet metal forming. Section 3 describes the experimental and numerical methods used in the study. In Section 4, we present the identification method and the results obtained. Section 5 discusses the validation of the identified models using hydroforming applications. Lastly, Section 6 summarizes the main findings of the study and provides directions for future research. The aim of this paper is to characterize and simulate forming

processes. We are particularly interested in developing a robust procedure for identifying the hot forming properties of thin structures using multiple regression techniques. Through the applications carried out, we are attempting to exploit multiple regressions and analysis of variance to describe an identification approach based on a limited number of simulations and experimental tests.

After identifying the behavior model parameters, the results obtained are used to study the plastic instability of S235.

## 2. Methods and materials

### 2.1. Behavior models

In a previous study, we established the relationships expressing the quadratic criterion HILL 48 coupled to isotropic ductile damage represented by the scalar $D$:

- The equivalent stress $\sigma_{eq}$ of HILL48:

$$\sigma_{eq} = \sqrt{F\sigma_2^2 + G\sigma_1^2 + H\left(\sigma_2 - \sigma_1\right)^2 + 2N{\sigma_{12}}^2} \,. \quad (1)$$

-The damage $D$ in terms of the cumulated equivalent plastic strain $\varepsilon_{eq}$

$$D = \left[\left(\varepsilon_{eq} + \varepsilon_s\right) / \varepsilon_u\right]^{\gamma} . \quad (2)$$

- The Swift model coupled to the damage:

$$\sigma_y = K\left[1 - D\right]\left(\varepsilon_0 + \varepsilon_{eq}\right)^n . \quad (3)$$

Two groups of parameters were determined to identify the behavior of the material: the first group includes the hardening parameters $K$, $\varepsilon_0$ and $n$, and the second group the damage parameters $\gamma$, $\varepsilon_s$ and $\varepsilon_u$ where $K$ (strength coefficient), $n$ (strain-hardening exponent), $\varepsilon_0$ (elastic strain to yield)

### 2.2. Multiple regression method

The problem is based on response variables $z_1$, $z_2$, …, $z_p$ and an influencing factor $x$ whose multiple regression leads to a relation of the form:

$$x = a_0 + a_1 z_1 + a_2 z_2 + \ldots + a_p z_p + \varepsilon \,, \quad (4)$$

where $a_0$, $a_1$, $a_2$, …, $a_p$ are the coefficients of the regression, $\varepsilon$ is an error.

To validate the quality of the regression equation between the influence factor and the response variables, we use the multiple determination coefficient defined by Eq. 5, where $SCR$ and $SCT$ are the squared sums of deviations:

$$R^2 = \frac{SCR}{SCT} \,. \quad (5)$$

### 2.3. Identification method

The multiple regression method is a statistical technique used to estimate the relationship between a dependent variable and multiple independent variables at the same time. The aim of this method is to identify the parameters that are significant for predicting the dependent variable.
The steps to perform a multiple regression are as follows:

- Data Collection: collect data on the independent and dependent variables.
- Data Analysis: analyze the data using graphs and statistics to understand the relationship between the variables.
- Model Construction: determine the variables that have a significant impact on the dependent variable. Construct a multiple regression model using these variables.
- Model Evaluation: evaluate the model using measures such as the coefficient of determination $R^2$ and residual analysis to determine the accuracy of the prediction.
- Interpretation of Results: interpret the results of the model to understand the relationship between the variables and to predict the dependent variable based on the values of the independent variables.

The parameters that are significant for predicting the dependent variable can be identified by examining the regression coefficients of the model. The regression coefficients represent the relationship between each independent variable and the dependent variable. Coefficients that have a significant t-value indicate a significant relationship between the corresponding independent variable and the dependent variable.

The identification method using the multiple regressions and analysis of variance is developed in two stages, as illustrated in the flowchart shown in Fig. 1.

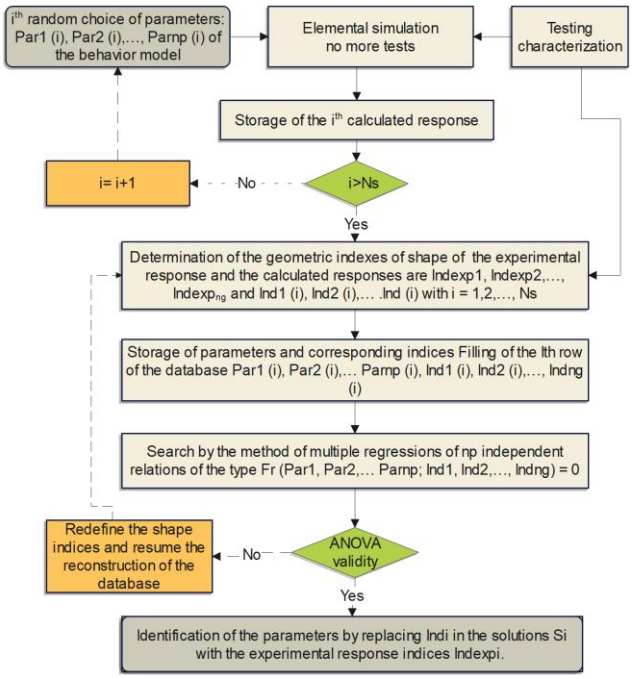


Fig. 1 Identification method using multiple regression

### 2.4. FE modeling and numerical simulations

The geometric model employed is a thin circular sheet with a diameter of 320 mm and thicknesses of 0.6 mm and 0.8 mm, respectively. The model is discretized utilizing hexahedral 3D solid elements with reduced integration and eight nodes (C3D8R). A total of 6552 elements are used in a two-zone meshing approach: the central region of interest adopts a fine mesh discretization while in the outer region,

a coarser mesh is used for computational efficiency (Fig. 2). This selective mesh refinement focuses computational resources on obtaining an accurate solution in the critical bulging area of the sheet.

The clamping area which anchored the sample was meshed with a course 10 mm x 2 mm brick element size for computational efficiency, yielding an aspect ratio of 5:1.

In the active bend zone of the sample, element sizes smoothly grade from 11 mm x 10 mm down to 2.3 mm x 2.3 mm moving through the bend region. Resulting aspect ratios range from 1.1:1 near the clamps up to 3:1 at the inner tensile edge. The central zone 42 mm diameter is discretized using elements with aspect ratios from 1.4:1 to 1:1.

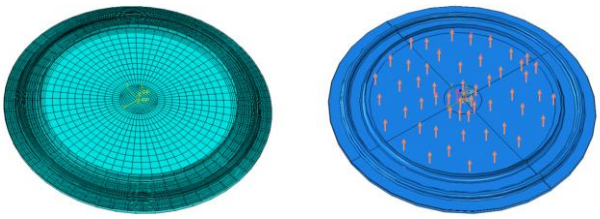

a b

Fig. 2 modeling numerical of bulge test: a - Test specimen meshing; b - loading conditions for the bulge using a circular die

The sheet is blocked between the die and the blank holder (Fig. 3). The circular die has an inside diameter of 220 mm with a fillet radius of 6 mm. It is modeled by shell elements R3D4, supposedly rigid and non-deformable. The Coulomb coefficient of friction between all the solids in contact is taken 0.1.

The boundary conditions (Fig. 3) consist of an embedding imposed on the matrix and a linear pressure exerted *Pmax* = 5 MPa on the blank according to the material to be tested.

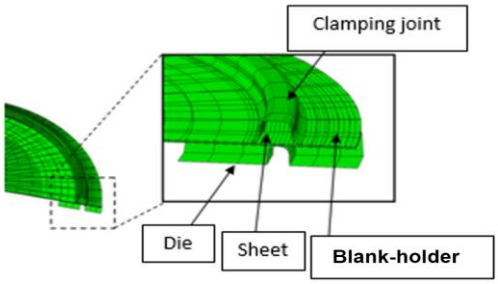


Fig. 3 Clamping of the sheet between the die and the blank holder

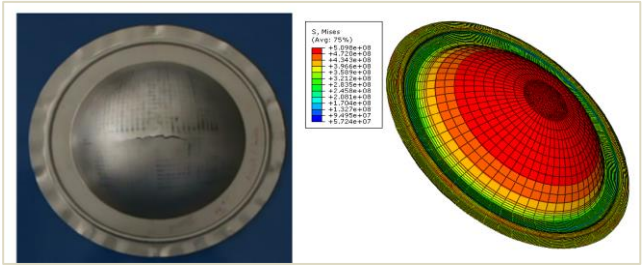

a b

Fig. 4 Bulge test pressure at the pole: a - experimental, b - simulated results

The data used to determine the identification procedure were obtained from hydraulic bulge tests on circular sheets 0.6 mm thick and having an active part with a diameter of 220 mm (Fig. 4).

## 3. Results and discussion

### 3.1. Identification of the work hardening parameters

The experimental shape indices of work hardening are the slope of the linear curve $a_e$ and the linear curve's intercept at the origin of the regression line $\Delta_e(a_e, b_e)$ (Fig. 5).

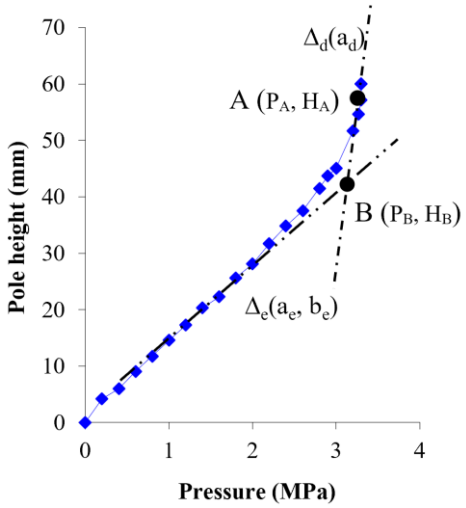


Fig. 5 Experimental shape indices for the identification of work hardening and damage of bulge test

The experimental damage shape indices $P_A$, $H_A$, $P_B$, $H_B$, $a_e$, $a_d$ are defined from the coordinates of the points *A*, *B* and the slopes of the two straight lines $\Delta_e$ and $\Delta_d$. Point $A(P_A, H_A)$, which corresponds to the maximum pressure, represents the point of the tangent to the line $\Delta_d$. Point $B(P_B, H_B)$ corresponds to the intersection of the two straight lines $\Delta_e$ and $\Delta_d$.

The first step was reserved for identifying the Swift model hardening parameters ($D = 0$; Eq. (3)), where the parameters $K$, $\varepsilon_0$ and $n$ were taken as influencing factors. In the second step, we were interested in identifying the damage parameters relating to the coupled Swift model ($D \neq 0$; Eq. (3)) where the parameters $\gamma$, $\varepsilon_s$ and $\varepsilon_u$ were taken for factors of influence.

Tensile tests oriented at 0°, 45°, and 90° to the rolling direction of E24 (S235) steel sheets were carried out to characterize the anisotropy (Table 1). The hardening parameters $K$, $\varepsilon_0$ and $n$ were taken as influencing factors. Indeed, the idea behind this new approach consists in executing successively until the identification of the work hardening parameters, numerical simulation factorial experimental plans ($v3 = k$ simulations) for the three factors of influences $K$, $\varepsilon_0$ and $n$ having progressive levels $v = 2, 3, 4, \ldots$ ($2^3$, $3^3$…). Table 2 presents the values of the potential levels of the parameters of hardening to be exploited in this step.

In this first step, the simulation plan $P^3(3^3)$, presented in Table 2, was sufficient to identify the hardening model parameters. The levels of each parameter are chosen based on published results.

Table 1
Parameters of Hill48 and mechanical properties of Steel S235 sheets

| Lankford coefficients | | | Anisotropy coefficients | | | |
|---|---|---|---|---|---|---|
| $r_0$ | $r_{45}$ | $r_{90}$ | $F$ | $G$ | $H$ | $N$ |
| 1.985 | 1.234 | 1.637 | 0.45 | 0.38 | 0.62 | 1.345 |
| Mechanical properties | | | | | | |
| Modulus of elasticity, GPa | | | Poisson's ratio | | | |
| 210 | | | 0.33 | | | |

Table 2
Values of the levels of the work hardening influence factors

| Influence factors | Label | Levels factors | | |
|---|---|---|---|---|
| | | 1 | 2 | 3 |
| Strength coefficient, MPa | $K$ | 400 | 500 | 700 |
| Initial strain, % | $\varepsilon_0$ | 1 | 2 | 3 |
| Hardening exponent | $n$ | 0.1 | 0.2 | 0.3 |

According to the ANOVA analysis of the simulated responses, the relations between the hardening parameters, where $x_q = K$ or $\varepsilon_0$ or $n$ and the shape indices ($a$ and $b$, respectively, the slope and the intercept of $\Delta_{ec}$) were determined according to the linear regression Eq. (6).

$$x_q = a_0 + a_1\delta_E + a_2 F_E \,. \qquad (6)$$

The values of the regression coefficients ($a_0$, $a_1$, and $a_2$) are obtained using the "LinearModel.stepwise" function in MATLAB©, which creates a linear model of the response $x_q$ as a function of the data matrix $Z$ (Eq. (4)) introduced, using stepwise regression to add or remove predictor variables (shape indices).

Table 3 presents the regression coefficients ($a_0$, $a_1$, and $a_2$) obtained for each of the simulation plans, for the parameters $K$, $\varepsilon_0$ and $n$ respectively, as well as the determination coefficients $R^2$ and $R^2_{adj}$, which make it possible to judge the quality of the linear regression relations.

The standard error (*RMSE*) is presented, which measures the deviation of the actual value from the regression prediction.

Table 3
Multi-linear regression coefficients of the work hardening parameters P ($3^3$)

| Coefficients | $K$, MPa | $\varepsilon_0$, % | $n$ |
|---|---|---|---|
| $a_0$ | 868.18 | 0.2 | 0.033191 |
| $a_1$ | -196.42 | - | 0.08245 |
| $a_2$ | 8.033 | - | 0.023253 |
| $R^2$ | 90.7% | - | 85.8% |
| $R^2_{adj}$ | 89.9% | - | 84.7% |
| *RMSE* | 39.6 | - | 0.0326 |

According to Table 3, the initial strain $\varepsilon_0$ does not depend on the shape indices. It is an equivalent strain from which work hardening is activated; it is considered an intrinsic parameter of the material, which remains constant.

The determination coefficients show that the linear regression relations obtained make it possible to explain more than 90% and 85% of the total variance of the hardening modulus $K$, the initial strain, and the hardening coefficient $n$ (Table 4), respectively.

Table 4
Experimental shape indices of the experimental bulge test

| $a_e$ | $b_e$ |
|---|---|
| 1.4841 | - 0.4755 |

The predictions of the uncoupled Swift model identified, and the experimental measurements of the hydraulic swelling test fit very well. The relative error between the experimental and numerical responses shows the quality of the results ($\xi_F$ =1.2%; Table 5; Fig. 6).

Table 5
Identification of hardening parameters

| Experiment design | $K$, MPa | $\varepsilon_0$, % | $n$ | $\xi_F$, % |
|---|---|---|---|---|
| $P(3^3)$ | 572.85 | 0.02 | 0.145 | 1.2 |

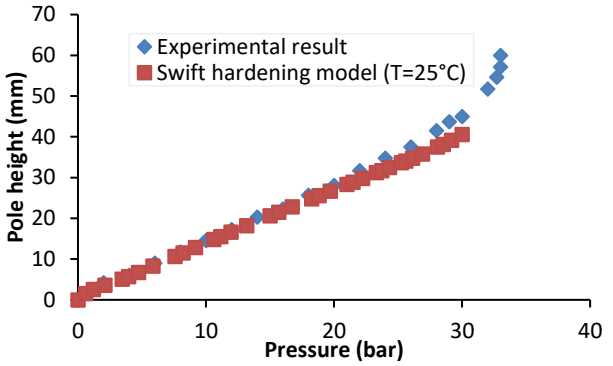


Fig. 6 Experimental and numerical responses for the Swift hardening model: height at the pole/ pressure of the bulge test

3.2. Identification of damage parameters

The parameters, damage threshold $\varepsilon_s$, cumulative total plastic strain $\varepsilon_u$, and damage indicator $\gamma$ characterized the ductile damage and were taken as influencing factors. Indeed, the idea behind this new approach consists in successively executing, until the identification of the damage variables, numerical simulation experiment design ($v^3 = k$ simulations) for the three influence factors ($\varepsilon_s$, $\varepsilon_u$ and $\gamma$) having three levels $3^3$. Table 6 presents the values of the levels of the damage variables to be exploited in this study. The levels of each parameter are chosen based on published results. Also, Table 7 represents the indices of experimental forms relating to the zone of damage.

From the ANOVA analysis of the simulated responses, the relationships between the damage parameters were determined by the linear regression relationship (7). The coefficients are presented in Table 8.

$$x_q = a_0 + a_1 P_A + a_2 H_A + a_3 P_B + a_4 H_B + a_5 a_e + a_6 a_d \,. \qquad (7)$$

Table 9 shows that the damage threshold $\varepsilon_s$ does not depend on the shape indices. Indeed $\varepsilon_s$ is an intrinsic parameter of the material; it represents the equivalent strain from which hardening is saturated, and the damage is activated. The determination coefficients show that the linear

regression relations obtained make it possible to explain the 86.7% of the total variance for the cumulative plastic strain $\varepsilon_u$ and the 66.4% of the total variance of the damage indicator $\gamma$.

The two damage parameters ($\varepsilon_u$ and $\gamma$) are identified by introducing the experimental shape indices as variables in the linear regression relations (Table 9). The relative error between the experimental and numerical responses shows that the results are good ($\xi_F$ = 0.45%; Table 9).

Fig. 7 shows that the predictions of the coupled Swift model and the experimental measurements fit very well.

Table 6

Values of the influence factors levels

| Influence factors | Label | Levels factors | | |
|---|---|---|---|---|
| | | 1 | 2 | 3 |
| Damage Threshold, % | $\varepsilon_s$ | 0.5 | 0.625 | 0.75 |
| Cumulative plastic strain, % | $\varepsilon_u$ | 50 | 60 | 70 |
| Damage indicator | $\gamma$ | 5 | 7.5 | 9.5 |

Table 7

Experimental shape indices

| $A$ | | $B$ | | $\Delta_1$ | $\Delta_2$ |
|---|---|---|---|---|---|
| $P_A$, bar | $H_A$, mm | $P_B$, bar | $H_B$, mm | $p_1$, bar/mm | $p_2$, bar/mm |
| 33 | 57.15 | 28.70 | 33.16 | 1.099 | 5.58 |

Table 8

Linear regression coefficients of damage parameters

| Coefficients | $\varepsilon_s$, % | $\varepsilon_u$, % | $\gamma$ |
|---|---|---|---|
| $a_0$ | 0.012667 | 0.075478 | -184.24 |
| $a_1$ | - | - | - |
| $a_2$ | - | - | - |
| $a_3$ | - | - | 5.833 |
| $a_4$ | - | - | -1.7551 |
| $a_5$ | - | - | 3.6949 |
| $a_6$ | - | 0.1157 | - |
| $R^2$ | - | 86.7% | 66.4% |
| $R^2_{adj}$ | - | 86.2% | 62% |
| *RMSE* | - | 0.0309 | 1.15 |

Table 9

Identification of the damage parameters

| Experiment design | $K$, MPa | $\varepsilon_0$, % | $n$ | $\xi_F$, % |
|---|---|---|---|---|
| $P(3^3)$ | 1.2667 | 72.14 | 13.99 | 0.45 |

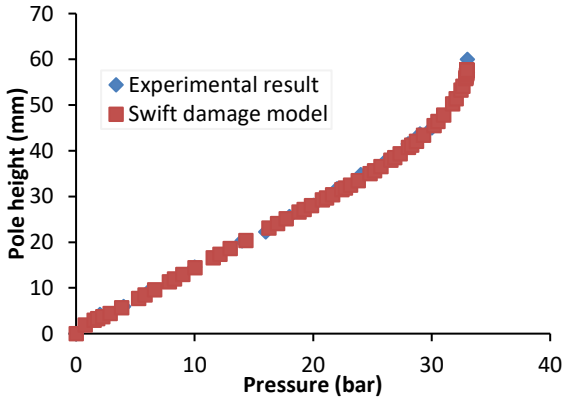


Fig. 7 Experimental and numerical responses of the Swift damage model: height at the pole/ pressure of the bulge test

## 3.3. Application of the identified models for the localization of instability areas

Two applications testing the elastoplastic behavior with considering the damage of the sheet have been developed to test the effectiveness of the identified models. The first concerned the expansion in a cavity of matrix CM (Fig. 8) made up of a succession of surfaces of revolution (conical, plane, spherical concave, and convex). The second relates to the free expansion of sheet metal with a set of blank holders SF1, SF2, SF3, SF4, and SF5 comprising square hollows with a side of 140 mm (Fig. 8). The blank holders are only distinguished by the radii of their fillets, fixed successively at 1.6, 2.2, 2.6, 2.9, and 3.6 mm.

The tests were carried out on circular plates (blanks) with a diameter of 300 mm and a thickness of 0.6 mm. The pressure applied to the blank is provided through a transmission fluid injected with a constant flow rate of approximately 10 ml/min. Numerical simulations of the same tests were carried out on Abaqus Implicit ©. The blank is assimilated to a deformable solid; its spatial discretization is carried out with hexagonal elements with reduced integration (C3D8R) and tetrahedral elements (C3D6). Their number is 4 144 for free expansion and 5 177 for expansion into the matrix cavity.

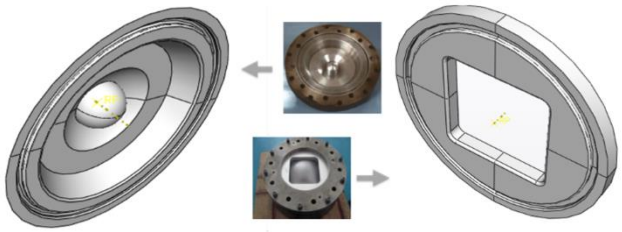

a b

Fig. 8 Blank-holder used in hydroforming applications: a - die cavity (CM), b - blank clamp with pseudo-square (SF) shape

### 3.3.1. Plastic instability criterion

In this section, the results of parameter identification of the Swift model coupled to damage are used to investigate the plastic instability of S235.

Swift criterion relating to the diffuse necking stipulates that the plastic instabilities appear when the load, along the principal directions, reaches the maximum. For a biaxial state of loading, the criterion is expressed by the relations between the stresses and the principal strains:

$$\frac{1}{\sigma_i}\frac{d\sigma_i}{d\varepsilon_i} = 1 \ (i=1, 2). \qquad (8)$$

When the co-axiality of the main axes and the orthotropy axes is verified, the diffuse necking criterion will then result in the following:

$$\frac{d\sigma_{eq}}{d\varepsilon_{eq}} = \sigma_1\left(\frac{\partial\sigma_{eq}}{\partial\sigma_1}\right)^2 + \sigma_2\left(\frac{\partial\sigma_{eq}}{\partial\sigma_2}\right)^2. \quad (9)$$

With a stress ratio:

$$\beta = \frac{\sigma_2}{\sigma_1}. \quad (10)$$

Eq. (9) becomes:

$$\frac{1}{\sigma_{eq}}\frac{d\sigma_{eq}}{d\varepsilon_{eq}} = \frac{\left(G^2+\beta^3F^2\right)+H^2(1+\beta)(1-\beta)^2+2H\left(G-\beta^2F\right)(1-\beta)}{\left(F\beta^2+G+H(1-\beta)^2\right)^{(3/2)}}. \quad (11)$$

Considering the expression of the coupled hardening law Eq. (3), the Eq. (11) reduces:

$$\frac{n}{\varepsilon_0+\varepsilon_c} - \frac{\gamma\left(\varepsilon_s+\varepsilon_c\right)^{(\gamma-1)}}{\varepsilon_u^{\gamma}-\left(\varepsilon_s+\varepsilon_c\right)^{\gamma}} = \frac{\left(G^2+\beta^3F^2\right)+H^2(1+\beta)(1-\beta)^2+2H\left(G-\beta^2F\right)(1-\beta)}{\left(F\beta^2+G+H(1-\beta)^2\right)^{(3/2)}}. \quad (12)$$

From the above equations, the plastic instability is determined using:

$$\varepsilon_1^c = \beta\varepsilon_2^c, \quad (13)$$

$$\varepsilon_2^c = \frac{n}{X}\left[\frac{\Omega}{\psi}-\frac{\varepsilon_0}{n}\right], \quad (14)$$

$$\sigma_1^c = \frac{\bar{\sigma}}{\bar{\varepsilon}}\left[\frac{(F+H)\varepsilon_1^c+H\varepsilon_2^c}{FG+FH+GH}\right], \quad (15)$$

$$\sigma_2^c = \frac{\bar{\sigma}}{\bar{\varepsilon}}\left[\frac{(G+H)\varepsilon_2^c+H\varepsilon_1^c}{FG+FH+GH}\right]. \quad (16)$$

Where $\varepsilon_1^c$, $\varepsilon_2^c$, $\sigma_1^c$ and $\sigma_2^c$ are the critical strains and stresses, respectively.

### 3.3.2. Zones of plastic instability onset in the matrix cavity subjected to bulge test

By adopting the analysis procedure based on evaluating the instability indicator, we could compare the experimental observations and the numerical simulations relating to hydroforming in a die cavity (first application). The main results are illustrated (Fig. 9, Fig. 10 and Fig. 10). It was also noted that the extreme values of the instability indicator produced by simulation are 0.96 for model 1 and 0.99 for model 2. These levels are reached with the respective pressures of 2.71 MPa and 3.17 MPa, respectively.

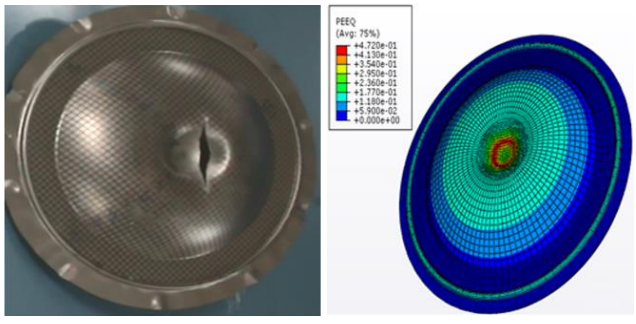


a b

Fig. 9 Location of damage and failure zones of blank under bulge test in the die cavity (a): failure of the test specimen, (b): localization of the failure zone by numerical simulation

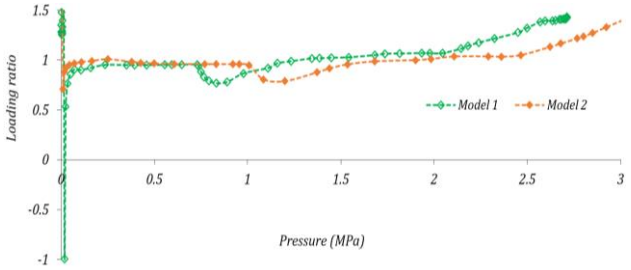


Fig. 10 Evolution of the loading ratio as a function of the pressure exerted on the blank

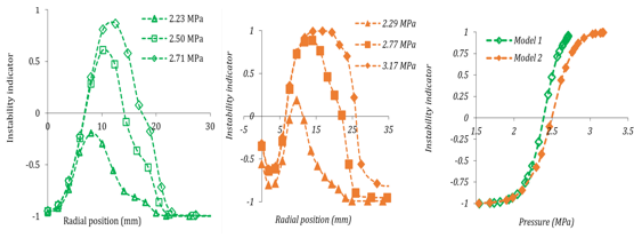


a b c

Fig. 11 Radial profiles and evolution of the instability indicator: a - prediction by model 1, b - prediction by model 2, c - evolution as a function of the pressure applied to the blank

### 3.3.3. Effect of the die's fillet radius

Fig. 12 shows that the blank's experimental deformation highlights the fillets' harmfulness when they encounter the sheet. For all the fillets admitting connection radii of less than 3.6 mm, the ruptures observed occurred in the areas of the smallest curvatures of the deformed sheet in contact with the blank holder. However, Fig. 13 shows a failure at the pole for the case of expansion in a blank holder with a 3.6 mm fillet radius. Some regions were subjected to a more in-depth analysis based on these observations. These are the pole and the contact areas between the blank and the fillets. In these two regions, which are at risk of rupture, it

is shown that if the pressure exerted on the blank shows exceeds 0.62 MPa, the condition relating to the proportionality of the loading is verified. Prediction results allow to track the evolution of plastic instabilities at the pole and the fillets were utilized based on these observations.

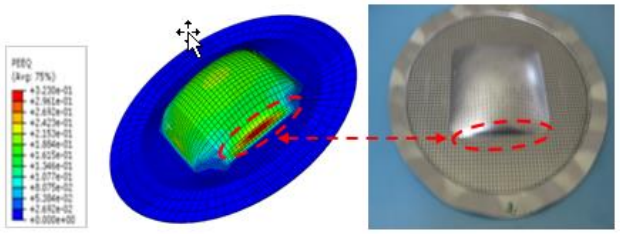

a b

Fig. 12 Location of damage and failure at the fillet (expansion with blank clamp SF1: radius fillet 1.6 mm): a - Numerical result; b - Experimental result

3.3.4. Estimation of the instability initiation pressure

On the diagrams expressing the instability indicator as a function of the pressure exerted on the blank (Fig. 13), it is possible to extract the pressures leading to the onset of the first instabilities ($\zeta = 0$) noted $P_a$, as well as the one corresponding to the maximum value of the indicator $\zeta_{max}$, noted $P_m$.

Fig. 14 summarizes the simulation results. It makes it possible to compare, for the two behavior models, the pressures of priming the plastic instability with the experimental pressures at rupture. The plastic instability onset pressures at the pole and the maximum pressures are not sensitive to changes in the radius of the blank holder fillet. At the level of the fillets, these pressures undergo an increase associated with an increase in the radius, followed by an asymptotic trend showing the existence of a critical radius above which the singularity no longer has any effect on the evolution of the instability indicator. These radii are estimated at 2.7 mm for model 1 and 3.1 mm for model 2.

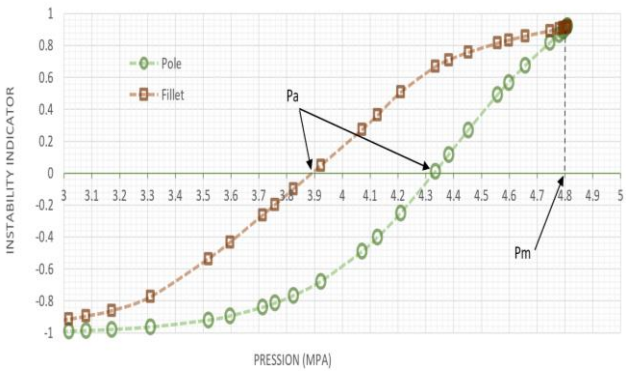


Fig. 13 Critical pressures from instability indicator diagrams (prediction of model 2 with the blank-holder SF1)

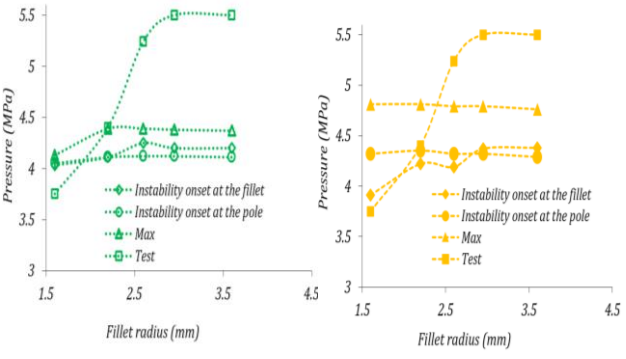


a b

Fig. 14 Critical and experimental failure pressures for the two predictive models: a - model 1; b - model 2

Moreover, the ruptures observed seem to correspond to the regions admitting the least onset pressures. This means that the expanding regions that are affected by the first instabilities can be correlated with the rupture zones. The severity of the instability can be correlated with the slope of the instability indicator/loading curve. It is also noted that the priming pressures are lower than the experimental rupture pressures, with a relative difference varying between 6.5% and 24%.

## 4. Conclusions

The investigations carried out in this study show the possibilities that the statistical analysis of simulation results can offer in terms of identification.

The performance of the method is linked to the initiation of the levels of influencing factors that will allow rapid convergence toward the optimum parameters. The initiation problem was avoided by establishing a factorial design of experiments sweeping a range of levels justified by the literature. We established a relationship between the material parameters and the experimental shape indices through a finite and organized number of simulations. Indeed, this method based on ANOVA and multiple regression allowed quick and efficient identification. This method could have great potential in computation time and result quality applied to other characterization tests. In addition, the formulations retained for identifying behavior models can be generalized to models with the same global behavior.

The identified models associated with the SWIFT diffuse necking criterion could be used to trace the critical deformation revealing the onset of the first instabilities. The introduction of the instability indicator, based on a measurement of plastic deformation and an evaluation of the loading ratio, makes it possible to locate areas at high risk of failure. The applications developed have also shown that the pressure priming instability is lower than the experimental rupture pressure, and the relative deviation varies between 6 and 24%.

In addition, the developed calculations have shown that the areas affected by the first instabilities are regions with a high risk of rupture when subjected to an evolutionary expansion loading. When these regions get stuck against the matrix wall, the development of instabilities can be stopped. The damage thus spreads to expanding areas directly affected by the combined effects of thinning and rising loading levels.

The study highlighted the potential offered by the multiple regression method in identifying models. It showed the validity of the method for analyzing sheet metal forming abilities through a confrontation with the Simplex method.

**Acknowledgements**

The authors gratefully acknowledge the approval and the support of this research study under the grant No. ENGA-2022-11-1928 from the Deanship of Scientific Research at Northern Border University, Arar, K.S.A.

**References**

1. **Gholami, D; Hashemi, M. R.; Sedighi, M.** 20209. The effect of temperature on the mechanical properties and forming limit diagram of aluminum strips fabricated by accumulative roll bonding process, Journal of Materials Research and Technology 9(2): 1831-1846. https://doi.org/10.1016/j.jmrt.2019.12.016.
2. **Wang, Q. L.; Novella, M. F.; Ghiotti, A.; Bruschi, S.** 2017. Anisotropy influence on flow behaviour and plastic instability of Ti6Al4V sheets deformed in a wide range of temperatures and strain rates, Procedia Engineering 207: 2161-2166. https://doi.org/10.1016/j.proeng.2017.10.975.
3. **Alizad-Kamran, M; Hoseinpour Gollo, M; Hashemi, A; Seyedkashi, H. S. M.** 2017. Determination of critical pressure in analyzing of rupture instability for hydromechanical deep drawing using advanced yield criterion, Archives of Civil and Mechanical Engineering 18(1): 103-113. https://doi.org/10.1016/j.acme.2017.05.008.
4. **Zhao, J; Jiang, Z; Wang, Z; Sang, S; Dobrzański, L. A; Yang, M; Ma, X; Wang, Y.** 2022**.** An analysis of micro deep drawing of ferritic stainless steel 430 using crystal plasticity finite element method, Journal of Materials Research and Technology 20: 2247-2261. http://dx.doi.org/10.1016/j.jmrt.2022.07.105.
5. **Wu, H; Zhuang, X; Zhang, W; Zhao, Z.** 2022. Anisotropic ductile fracture: experiments, modeling, and numerical simulations, Journal of Materials Research and Technology 20: 833-856. https://doi.org/10.1016/j.jmrt.2022.07.128.
6. **Barrett, T. J.; Knezevic, M.** 2019. Deep drawing simulations using the finite element method embedding a multi-level crystal plasticity constitutive law: Experimental verification and sensitivity analysis, Computer Methods in Applied Mechanics and Engineering 354: 245-270. https://doi.org/10.1016/j.cma.2019.05.035.
7. **Chen, K; Korkolis, Y.P.** 2020. Industry 4.0 in stamping: A wrinkling indicator for reduced-order modeling of deep-drawing processes, Procedia Manufacturing 51: 864-869. https://doi.org/10.1016/j.promfg.2020.10.121.
8. **Amaral, R; Santosa, A. D.; Lopes, A. B.** 2017. Mechanical properties determination of dual-phase steels using uniaxial tensile and hydraulic bulge test, Ciência & Tecnologia dos Materiais 29(1): e239-e243. https://doi.org/10.1016/j.ctmat.2016.06.007.
9. **Sun, J; Nitschke-Pagel, T.; Dilger, K.** 2022. Influence of strain-hardening models and slopes on the predicted residual stresses in structural steel S235 weldments, Journal of Materials Research and Technology 19: 4044-4062. https://doi.org/10.1016/j.jmrt.2022.06.134.
10. **Zhang, B; Endelt, B; Nielsen, K. B.** 2022. Characterization of mechanical properties for tubular materials based on hydraulic bulge test under axial feeding force, Fundamental Research 3(4): 592-601. https://doi.org/10.1016/j.fmre.2022.01.024.
11. **Madani, T.; Boukraa, M.; Aissani, M.; Chekifi, T.; Ziadi, A; Zirari M.** 2023. Experimental investigation and numerical analysis using Taguchi and ANOVA methods for underwater friction stir welding of aluminium alloy 2017 process improvement, International Journal of Pressure Vessels and Piping 201, 104879. https://doi.org/10.1016/j.ijpvp.2022.104879.
12. **Hou Y, Myung D, Park JK, Min J, Lee HR, El-Aty AA, Lee MG.** 2023. A Review of Characterization and Modelling Approaches for Sheet Metal Forming of Lightweight Metallic Materials. Materials 16, 836. https://doi: 10.3390/ma16020836.
13. **Chen, K.; Scales, M.; Kyriakides, S.** 2018. Material hardening of a high ductility aluminum alloy from a bulge test, International Journal of Mechanical Sciences Volumes 138–139: 476-488. https://doi.org/10.1016/j.ijmecsci.2018.02.002.
14. **Badgujar, T. Y.; Wani, V. P.** 2017. Stamping Process Parameter Optimization with Multiple Regression Analysis Approach, Materials Today: Proceedings 5(2), Part 1: 4498-4507. https://doi.org/10.1016/j.matpr.2017.12.019.
15. **Ramanjaneyulu, P.; P. Venkataramaiah, Reddy, K. D.** 2019. Multi parameter optimization of deep drawing for cylindrical cup formation on brass sheets using Grey Relational Analysis, Materials Today: Proceedings v18, Part 7: 2772-2778. https://doi.org/10.1016/j.matpr.2019.07.142.
16. **Bashah, N. A. K.; Muhamad, N.; Deros, B. M.; Zakaria, A.; Ashari, S.; Mobin, A.; Lazat, M. S. M. A.** 2013. Multi-regression modeling for springback effect on automotive body in white stamped parts, Materials & Design 46: 175-190. https://doi.org/10.1016/j.matdes.2012.10.006.
17. **Guo, X.; Xu, H.; Zeng, Q.; Pet, T.** 2021. Springback characteristics of arched aluminum alloy gusset plate after stamping forming, Thin-Walled Structures 159, 107294. https://doi.org/10.1016/j.tws.2020.107294.
18. **Chen, W.; Li, S; Bhandari, K; S.; Aziz, S.; Chen, X.; Jung, D. W.** 2023. Genetic optimized Al–Mg alloy constitutive modeling and activation energy analysis, International Journal of Mechanical Sciences 244, 108077. https://doi.org/10.1016/j.ijmecsci.2022.108077.
19. **Ibragimova, O.; Brahme, A.; Muhammad, W.; Connolly, D.; Lévesque, J.; Inal, K.** 2022. A convolutional neural network-based crystal plasticity finite element framework to predict localised deformation in metals, International Journal of Plasticity 157, 103374. https://doi.org/10.1016/j.ijplas.2022.103374.
20. **Yao, D.; Yong-chuan, D., Mu-yu, Li; Ying-ping, G.** 2021. Hybrid identification method of coupled viscoplastic-damage constitutive parameters based on BP neural network and genetic algorithm, Engineering Fracture Mechanics 257, 108027. https://doi.org/10.1016/j.engfracmech.2021.108027.
21. **Zhou, T.; He, L.; Feng, Z.; Tian, P.; Du, F.; Zou, Z.; Zhou, X.** 2022. Inverse identification of material constitutive parameters based on co-simulation, Journal of Materials Research and Technology 20: 221-237. https://doi.org/10.1016/j.jmrt.2022.07.073.

N. Ghazouani, M. T. Nasri, B. Eladeb, W. Salah,
M. A. Tashkandi, N. Becheikh

THE CHARACTERIZATION OF THE PLASTIC INSTABILITY OF S235 THIN STEEL SHEETS BY MULTIPLE REGRESSION AND ANALYSIS OF VARIANCE METHODS

S u m m a r y

In this study, we present a new identification method of parameters characterizing the elastoplastic damage behavior of sheet metal based on analysis of variance. The analysis covered experimental and numerical simulation results using the finite element method of the sheet mild steel bulge test. The identification procedure was validated through a confrontation between numerical simulations and experimental results on several hydroforming applications, such as a free expansion and an expansion in matrix cavities. Results show consistency between experimental observations and numerical predictions of instabilities. Furthermore, the location of risk areas of instability and rupture and the damage level could be quantified. The analysis focused on a set of results combining experimental data and numerical simulations of the bulge test of steel sheets. The identified models were validated thanks to a comparison between numerical simulations and experimental results of a set of forming applications by bulge test. The results show coherence between the experimental observations and the numerical predictions of the instabilities.

**Keywords:** work hardening, damage, bulge test, analysis of variance, multiple regression.

Received May 5, 2023
Accepted February 15, 2024